STUDY OF RAPID SEDIMENTATION AT PARESAR INTAKE BASIN, CASPIAN SEA, DUE TO LARGE WRACK PARTICLES AND WIND-INDUCED CURRENTS

Mina Rashvand[1], Mohsen Soltanpour[2] and Amir Masoud Moattar Kharrazi[3]

The rapid sedimentation at the entrance of Paresar intake basin is studied, in which unnatural wracks accumulation at the coast, combined with the existing sand, resulted in a major increase in the actual Longshore Sediment Transport (LST) rate. Considering the volume of updrift fillet at the northwest of the main breakwater and the estimated LST rate, the rapid advancement of the updrift shoreline was highly unexpected. Sands and vegetative wracks were observed only three years after the construction of the rubble mound breakwaters of the intake, resulting in water depth decrease at the basin entrance. Employing field measurements and numerical modeling, it was revealed that general wind-induced currents in the Caspian Sea, which were ignored in the design phase, have a small effect on increasing the LST rate. The unusual sedimentation can be mainly related to the high percentage of wrack particles at the updrift coasts.

Keywords: Paresar intake basin, sedimentation, wind-induced current, wrack particles, longshore sediment transport

INTRODUCTION

The construction of coastal structures, such as groins and breakwaters, generally results in an extensive shoreline change. The blockage of Longshore Sediment Transport (LST), i.e. the cumulative movement of nearshore sand parallel to the shore, is the common reason of shoreline advancement and retreat at updrift and downdrift sides of coastal structures, respectively.

CERC formula (USACE, 1984), which relates the potential LST rate to the longshore wave energy flux, has been widely used to estimate the LST rate for many years. Including the effects of bottom slope, grain size, and wave period, Kamphuis (2002) presented another 1D formula for the prediction of the LST rate. However, these simple formulas, which ignore important inputs such as particle fall velocity, sediment density, shields parameter, and cross-shore bed profile, may considerably differ from the actual LST rate. The complex details of sediment transport is an ongoing research with many unknown involved phenomena and a fully 3D numerical model has not yet been developed (Fredsøe and Deigaard 1992).

STUDY AREA

Caspian Sea is the largest inland water of the world with an area of about 371,000 km^2, excluding the Kara-Bogaz-Gol Bay. Paresar power station is located in the southwest of the Caspian Sea in Gilan province of Iran (Fig. 1). The coastal works consisted of building a sheltered basin (with two rubble mound breakwaters) for the intake of cold water, a discharge cannel for returning the warm water back to the Caspian Sea and pumping station. After the construction of breakwaters in 2007, large volumes of sand and vegetative wracks resulted in a rapid shoreline advancement behind the main breakwater. Comparing the hydrography surveys of 2007 and 2012, it was concluded that the actual LST rate is much more than the estimated design value. Fig. 2 presents the LST direction and the diffraction current at the downdrift side of the basin, considering the wave rose.

From July 2012 to December 2013, the rapid sedimentation and advancement at the updrift shoreline resulted in a decrease of water depth at the entrance of basin and sediment was finally observed in the basin in March 2014. Fig. 3-a and 3-b show the developed beach at updrift coast, i.e. northwest of the main breakwater. A small crenulated-shape beach, due to diffraction current, can be observed at the south of the secondary breakwater too (Fig. 3-c).

FIELD AND LABORATORY EXPERIMENTS

The data of waves and currents were selected from extensive field measurements at south Caspian Sea, including existing buoys and installed Acoustic Doppler Current Profilers (ADCPs) by the Iranian Ports and Maritime Organization (PMO) of Iran in 2013. The authors also conducted a series of field surveys at the site in September 2016, with the aim of coastal reconnaissance. These surveys include visual observation of adjacent rivers and estuaries, both in nearby northwestward and southeastward coasts of the basin, sediment sources, and clues of morphological evidences to confirm the direction of LST. Sediment samples were also taken from the dug trenches at updrift advanced shore of the main breakwater at different depths (Fig. 4). The samples were sealed off in zip-lock plastic bags to ensure no moisture loss. The hydrological data and surveys showed that the large number of small rivers in updrift side of the intake, as well as the mountainous and steep slopes of western Gilan Province, are the cause

[1] Formerly, Civil Engineering Department, K. N. Toosi University of Technology, No. 1346, Vali-Asr St., Tehran, Iran
[2] Civil Engineering Department, K. N. Toosi University of Technology, No. 1346, Vali-Asr St., Tehran, Iran
[3] Civil Department, MAPNA Combined Cycle Power Plants, Construction & Development Co. (MD-2), No.250, Africa Ave., Haghani Crossroads, Tehran, Iran

and source of the large vegetative wracks at the coast. The wracks are mainly transported to the river estuaries by floods during winter storms.

Figure 1. Paresar power station in south coast of Caspian Sea (left) with huge wrack particles at the updrift coast (right).

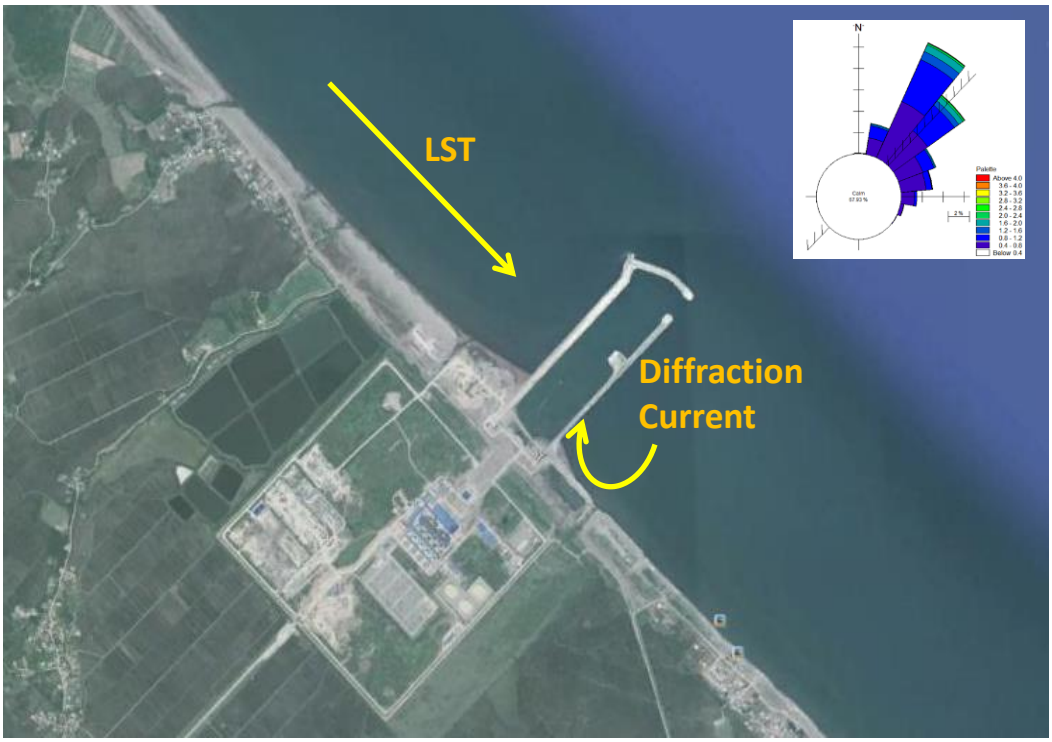

Figure 2. Deep water wave rose, LST direction and diffraction current.

Figure 3. Sedimentation in front of the main breakwater (a-b) and behind the secondary breakwater (c).

Figure 4. Mixed sand-wrack layers at four dug trenches in the updrift fillet of the basin.

The wrack particles were detached from sand to determine their physical properties, including particle size, relative density, and porosity. Table 1 presents the bulk properties of sediment samples and wrack particles. The common method of sieve analysis was used to define particle size distribution of sand particles. Volume-based particle size d_e, i.e. the diameter of the sphere that has the same volume as the given wrack particle (Fredsøe and Deigaard 1992), was employed for non-spherical wrack particles, which cannot be analyzed using a sieve (Clift 2005). The equivalent diameter is defined through

weighing a counted number of particles from a certain fraction of the sample. Fig. 5 shows the particle size distributions of wrack and sand particles, taken along the cross-shore profiles of updrift and downdrift coasts (A1: water depth of -4 m to -15 m, A2: water depth of -2.5 m to -4 m, A3: water depth of -2.5 m to -1 m, A4: water depth of -1 m to elevation of +5 m).

Table 1. Properties of sediment samples and wrack particles

	Bulk density	Dry density	Relative density	Mass ratio (*w*/*s*)
wrack+sand	1.235 1.027 1.165	-	-	0.53 0.58 0.55
wrack	-	0.405 0.343 0.387	1.1-1.2	

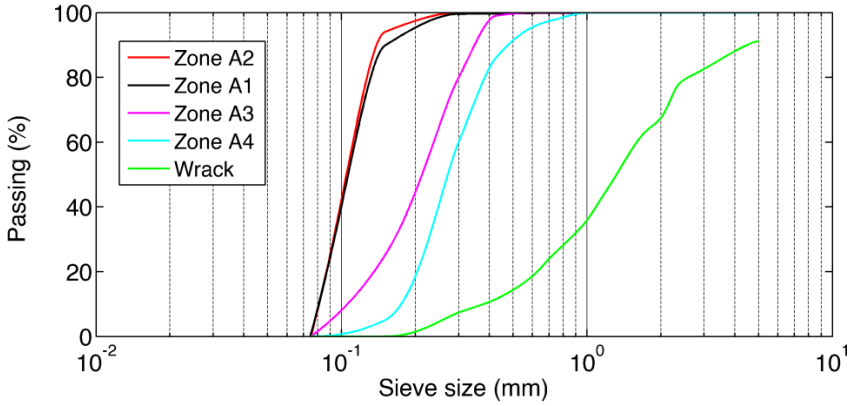

Figure 5. Distributions of wrack and sand particles at different zones along the cross-shore profile (Data of zones 1 to 4 was adopted from SPI 2007).

NUMERICAL MODELING

Using the numerical outputs of velocity field to force the wrack particles, a Lagrangian based particle-tracking model is needed to simulate the wracks transport towards the basin (Oldham et al. 2010). The blocked accumulated wracks by the main breakwater can then be added to the sand deposition to get the total sediment accumulation and the consequent shoreline change. In this study, the sand-wrack mixture was treated as a mixed coarse sediment. This simplified assumption might be justified considering that the bed load is much smaller than the suspended load in the present modeling of sand sediment transport. The parameters of the mixed sand-wrack are defined in a way that do not violate the boundaries of input parameters of the sand transport model. Models developed by Danish Hydraulic Institute (DHI) are used for the numerical modeling of the waves, currents, sediment transport and morphology.

Based on equivalent diameter and density of particles, the general formula of Ruby (1933), which is not exclusive to sand particles, was adopted between the existing formulas of particle fall velocity:

$$w_s = \sqrt{g(s-1)d}\left[\left(\frac{2}{3}+\frac{36\vartheta^2}{g(s-1)d^3}\right)^{1/2}-\left[\left(\frac{36\vartheta^2}{g(s-1)d^3}\right)^{1/2}\right]\right] \quad (1)$$

where w_s is particle fall velocity, s is the relative sediment density, g is the gravitational constant, d is the particle diameter, and ϑ is kinematic viscosity.

Sheilds number is another important parameter in numerical modeling of sand-wrack mixture transport. Considering the type and geometry of particles, Eqs. (2) to (5) are respectively used to calculate the shields parameter (Le Roux 1998):

$$D_d = D\sqrt[3]{\rho g\frac{s-1}{\vartheta^2}} \quad (2)$$

$$W_{ds} = 0.2636D_d - 0.37 \quad (3)$$

$$W_{ds} = 0.0384{W_{dm}}^2 + 0.8575W_{dm} \quad (4)$$

$$\theta_c = -0.0321\, ln\, W_{dm} + 0.0655 \quad (5)$$

where D_d is dimensionless particle diameter, W_{ds} is dimensionless particle fall velocity due to sieve size, W_{dm} is dimensionless fall velocity of natural particles, and θ_c is particle shields parameter.

Wave Climate

Surface gravity waves in the south coasts of Caspian Sea are generated wind waves, mostly coming from the Northwest direction. Fig. 6 shows the eleven years (1992–2002) hindcast wave rose, adopted from Iranian Sea Wave Model (ISWM), in front of the Paresar intake (Golshani et al. 2007). It is observed that most waves are perpendicular to the shoreline, coming from the northwest. Small directional segments should be selected in numerical models to get the accurate wave transformation and longshore currents.

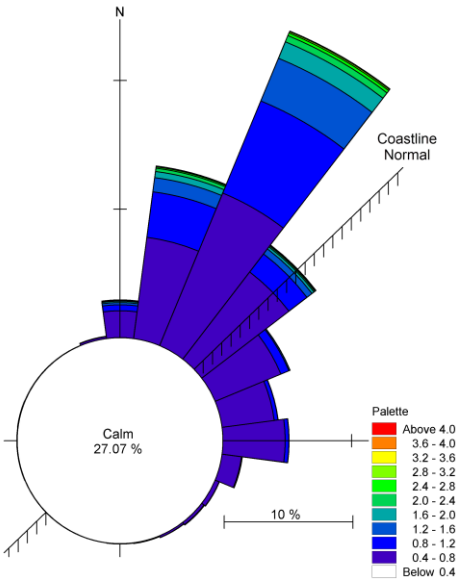

Figure 6. Deep water ISWM wave rose in front of the Paresar basin.

Currents

2D Flow Model of MIKE 21 was used to study the effect of wind-induced currents on LST rate. As the Caspian Sea is not connected to open seas, the currents are mainly governed by the winds, in the absence of meaningful tides (Bohluly et al. 2014). The other influencing factors, such as water temperature and density gradients, are normally less effective to generate the currents. Therefore, the sand and wracks are mainly transported towards Paresar basin by wind-induced currents and wave-induced longshore currents.

Fig. 7 presents the bathymetry and computational grids of 2D Caspian Sea flow model, with the total number of mesh = 63950, minimum element size = 50 m near the study area and maximum area of elements ~ 300 m^2. Wind input was extracted from the European Center for Medium-Range Weather Forecasts (ECMWF) data source with an accuracy of 0.125*0.125 deg. Using the calibrated Manning coefficient of 80, the 2D model was validated with the measured data at 10 m water depth in front of Astara Port. Fig. 8 presents 10-weeks comparisons of modeling results with monitoring data. The observed discrepancy can be related to relatively coarse mesh that was employed in Astara Port, about 100 kilometers far from the site. 3D behavior of the current and other factors, such as small variations of water temperature and density, also affect the numerical modeling results. The outputs of the 2D flow model show that in shallow waters, the current roses are unsurprisingly parallel to the shoreline. The outputs of the Flow model are imposed to the sediment transport model.

Sediment Transport and Morphology

The rate of longshore sediment transport and coastline evolution are determined by LITDRIFT and LITLINE of LITPACK Toolbox, respectively (DHI, 2012). The core of the sand transport calculations in the littoral processes is a Quasi Three-Dimensional Sediment Transport model (STPQ3D). STPQ3D model calculates instantaneous and time-averaged hydrodynamics and sediment transport in two horizontal directions at a given point.

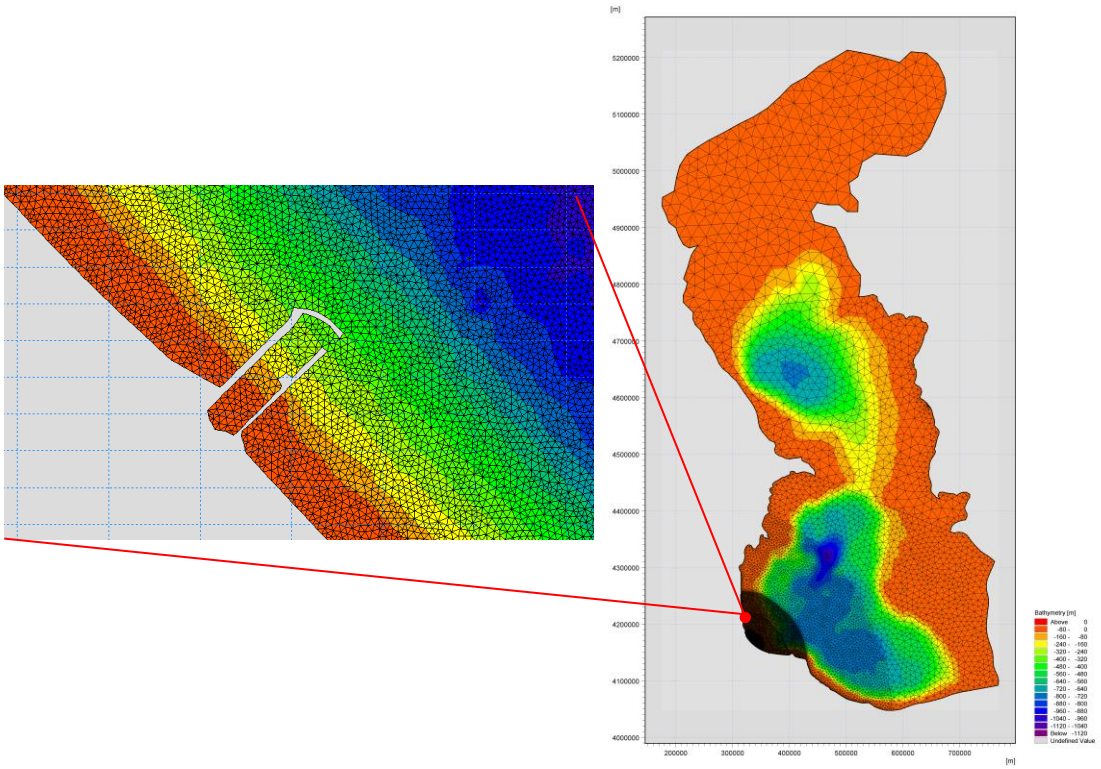

Figure 7. Bathymetry and computational grids of the Caspian Sea and study area.

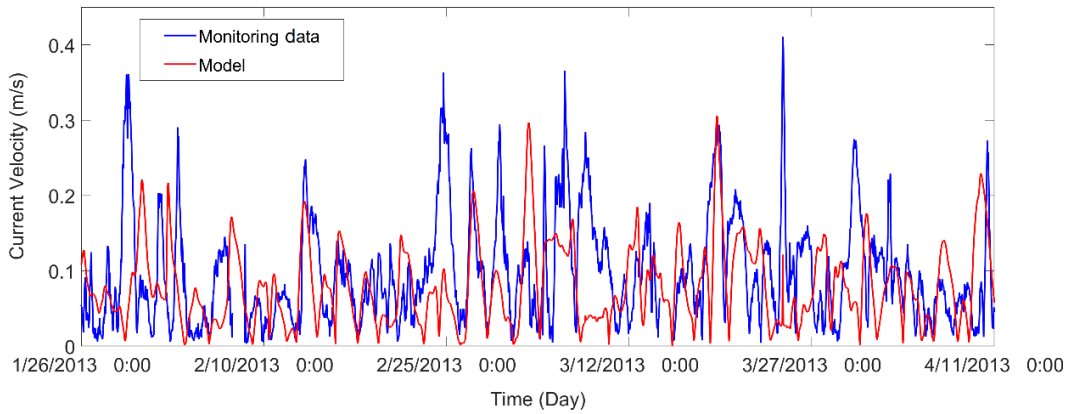

Figure 8. Comparisons between the data and simulated wind-induced currents in front of Astara Port.

The conducted hydrography surveys at the site, i.e. updrift of the main breakwater, show the maximum shoreline advancement of about 130 m after three years with a yearly average LST rate of about 100,000 m^3. Considering the basic assumptions of 1D modeling, i.e. a constant shape of cross-shore profile in longshore direction with similar sediment physical properties, Fig. 9 presents the initial cross-shore profile and mean diameters of sand particles in the model. The calibration parameters are the bed roughness coefficient and active depth, which are estimated as $200d_{50}$ and 6.5 m, respectively. It is necessary to include the effect of ripples on the bed in order to get correct bed shear stresses. Fig. 10 shows the model results of net annual drift and coastline evolution.

Using LITSTP module, a sensitivity analysis was also conducted to estimate the impact of physical properties of sediment on the transport rates of bed load and suspended load. This module can be applied for a specific point to study the sediment transport under the waves and currents. A sample high wave, coming from the dominant direction, was selected from the LITDRIFT module. Fig. 11 presents the wave transformation and selected red point on the sleep slope in the breaking zone. Table 2 offers the specifications of the point.

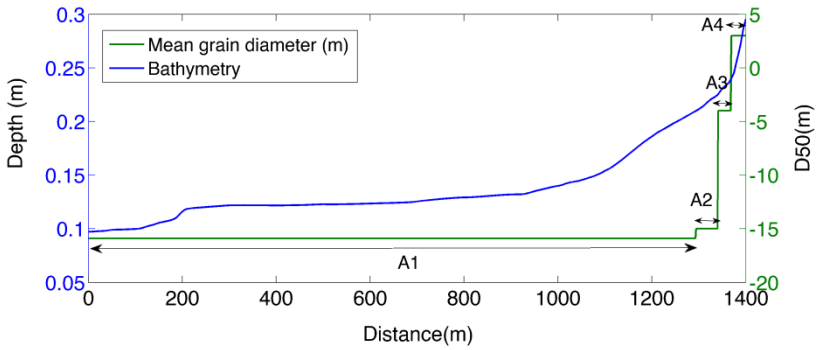

Figure 9. Initial cross-shore profile and mean diameters of sand particles at different zones of A1 to A4.

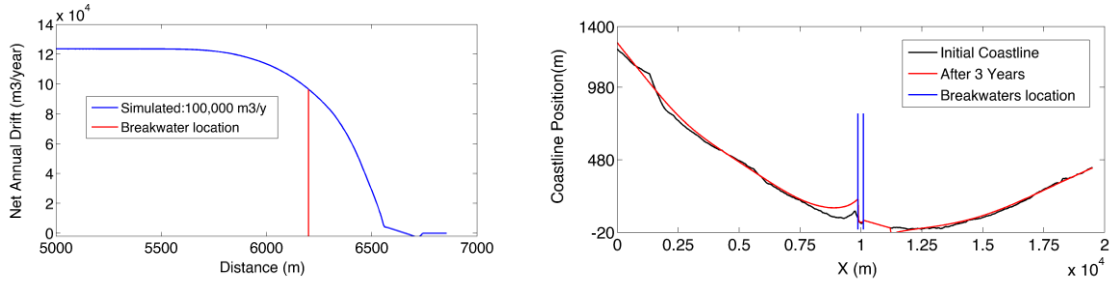

Figure 10. Modeled net annual longshore drift at the tip of main breakwater (left) and coastline evolution after three years (right).

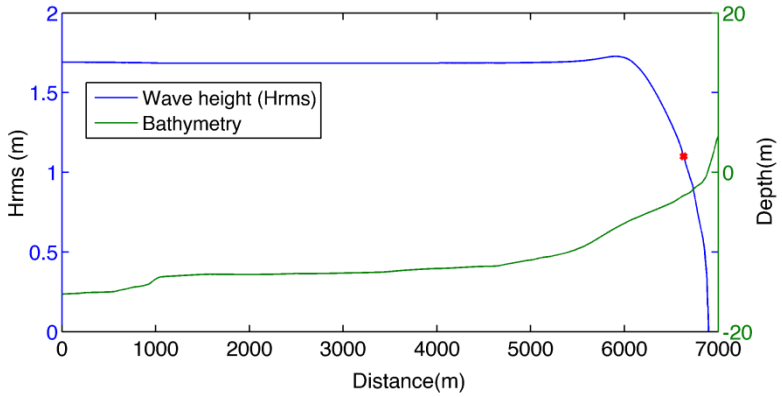

Figure 11. Wave transformation and location of selected point on cross-shore profile.

Table 2. Parameters of the selected point in the breaking zone.

Water depth (m)	H_{rms}(m)	Wave angle (deg)	Bed slope	D_{50} (mm)		Spreading factor		Critical shields parameter	
				sand	wracks	sand	wracks	sand	wracks
3	1.12	31.5	0.0073	0.1	0.12	1.22	1.6	0.045	0.06

Using the input parameters of Table 2, Fig. 12 presents sample outputs of the sediment model for sand and wracks. It is observed that the variations in particle size, porosity, density, and shields parameter significantly affect the sediment transport rate. Comparison between the deterministic and empirical approaches in defining the input parameters, it can be concluded that the shields parameter has a significant impact on the numerical results among the influencing factors. Although the employed method of simulating the transport of the sand-wrack mixture by LITPACK, originally developed for non-cohesive sediments with little organic materials, lacks a robust background support, it can approximately simulate the total transport, if important parameters are well defined and calibrated.

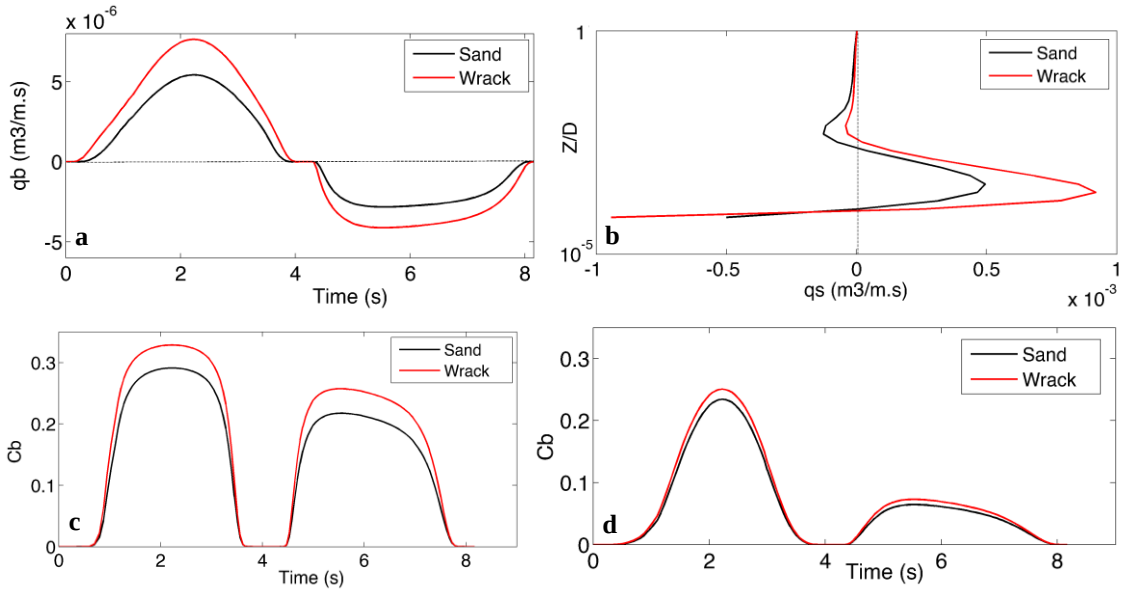

Figure 12. a) Bed load distribution, b) Suspended load distribution, c) Bed concentration (deterministic approach), d) Bed concentration (empirical approach).

RESULTS AND DISCUSSION

Fig. 13 shows the agreement of current velocity distributions across the cross-shore profile between 1D model of LITPACK and 2D Flow model. It is observed that the velocity distribution along the cross-shore profile follows the bed geometry, gradually decreasing to zero velocity at the shore.

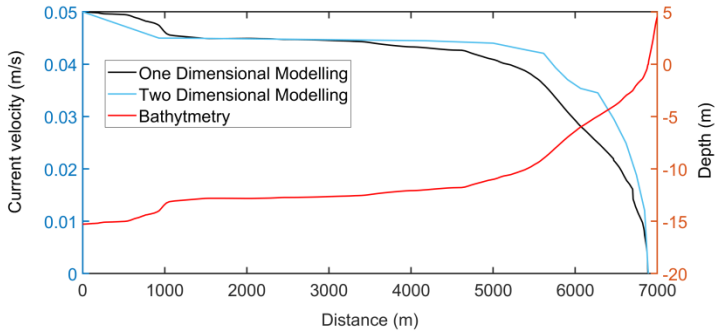

Figure 13. Comparison between current velocity distributions of 1D (LITPACK) and 2D (Flow) models.

Fig. 14 presents the accumulative effects of different factors on sediment rate and deposition at the basin entrance associated with time. The contribution of wind-induced current is not significant but the existence of wrack particles considerably increases the littoral drift and deposition at the entrance. However, wind and wind-generated currents can increase the dispersion and transport of suspended particles to deeper parts, resulting in reduction of water depth at the tip of the main breakwater. It is also observed that the contribution of wrack particles significantly increases the bypassing in a long time.

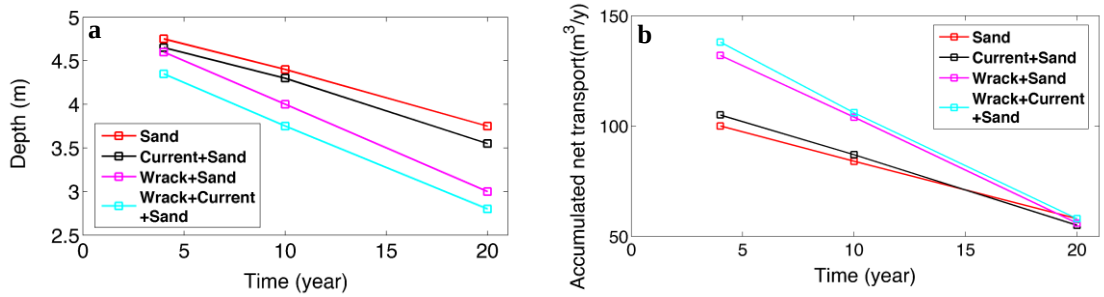

Figure 14. a) Combined effects of wind-induced current and wrack particles on water depth at the tip of main breakwater, b) Accumulated annual net sediment transport.

CONCLUSIONS

Similar to sand transport in littoral zone, the wracks are mainly transported along the beach, particularly during storm events, in response to the wave-induced longshore current. The main breakwater of the Paresar basin not only acts as a barrier to LST but also blocks the wracks movements along the shore. The mixture of sand and wrack particles, trapped at the northwest of the main breakwater of Paresar intake, has resulted in a rapid advancement of the shoreline, reducing the water depth at the basin entrance and endangering the necessary discharge of input water to the power station. The present study was aimed at improving the knowledge of increased littoral drift towards Paresar basin and consequent sedimentation at the entrance.

Changing the important parameters of sand, a simplified approach was adopted in numerical modeling of mixed sand-wrack, considering that the contribution of suspended transport is much higher than the portion of bed load in the total sediment transport. It was revealed that although the layout of breakwaters is adequate regarding the required calmness of the basin, it does not provide the necessary reservoir to trap the actual LST including wrack particles.

Different remedy solutions were examined to stop the sediments or mitigate the sedimentation at the basin entrance. Continuous periodic marine-based dreading was the first choice but it was rejected mainly because of the shortage of small dredgers, which highly increases the maintenance costs in long periods. A system of one or two groins, constructed at updrift side to block the LST before approaching the basin, together with one-time dredging of the basin entrance was also considered. This method can ensure the performance of the basin for a long time, i.e. before filling the fillets behind the proposed groins (Soltanpour et al. 2015). Moreover, it keeps the designed navigational depth at the basin entrance, which will be important for importing the machineries and materials, particularly if the construction of the next phases of power station starts. Hydraulic sediment bypassing was another attractive solution, specially because of the availability of electrical energy at the site.

As there was no urgent need to keep the navigation depth at the basin entrance, the continuous mechanical excavation at updrift fillet was found to be the most economical solution. Excavation and transport of the trapped sediment at updrift coast by mechanical shovels and trucks, was proposed as the best cost-effective solution. The volume of regular excavation need to be higher than the estimated rate of LST, i.e. about 100,000 m^3 per year. Considering the shortage of sand mines at North provinces of Iran, bordering the Caspian Sea, the excavated sand can be used in construction projects. Alternatively, it might be transported to the downdrift side of the basin to compensate the blockage of LST. This stops the erosion and retreat of shoreline in front of nearby downdrift villages. The proposed regular maintenance has been successfully employed at the site, resulting in the continuous operation of the power station in past few years.

ACKNOWLEDGEMENTS

The authors are grateful to the Construction & Development Co. (MD-2) of MAPNA Combined Cycle Power Plants for providing the field measurements and consultant design reports, logistical supports during field surveys and sediment samplings, and valuable discussions during this study. Thanks are also extended to the Directorate General for Coastal and Port Engineering of PMO for providing the data of “Monitoring and Modeling Studies of the Iranian Northern provinces coasts”.

REFERENCES

Bohluly A., Namin M.M., Teheri A.A., 2014. Simulation of wind-driven currents pattern in the Caspian Sea using PMODynamics, *11th International Conference on Coasts, Ports & Marine Structures, ICOPMAS*, 60-63.

Clift, R., Grace, J.R., Weber, M.E., 2005. Bubbles, drops, and particles. *Courier Corporation*, 381 pp.

Danish Hydraulic Institute (DHI), 2012. An integrated modeling system for littoral processes and coastline kinetics, User guide of LITPACK Toolbox, 66 pp.

Fredsøe, J., Deigaard, R., 1992. Mechanics of coastal sediment transport. *Singapore: World scientific*, 3, 369 pp. https://doi.org/10.1142/1546

Golshani, A., Taebi, S., Chegini. V., 2007. Wave hindcast and extreme value analysis for the southern part of the Caspian Sea, *Coastal Engineering Journal*, And 49 (04), 443-459. https://doi.org/10.1142/S057856340700168X

Kamphuis, J.W., 2002. Alongshore transport of sand. Proceedings of the 28th International Conference on Coastal Engineering, *ASCE*, 2330–2345.

Le Roux, J.P., 1998. Entrainment threshold of natural grains in liquids determined empirically from dimensionless settling velocities and other measures of grain size. *Sedimentary Geology*, 119, 17-23. https://doi.org/10.1016/S0037-0738(98)00022-0

Oldham, C.E., Lavery, P.S., McMahon, K., Pattiaratchi, C., Chiffings, T., 2010. Seagrass wrack dynamics in Geographe Bay, Western Australia. *Report to Western Australian Department of Transport, and Shire of Bussleton*, 214 pp.

Rubey, W.W., 1933. Settling velocity of gravel, sand, and silt particles. *American Journal of Science*, 148, 325-338. https://doi.org/10.2475/ajs.s5-25.148.325

Soltanpour, M., Sana, A., Baawain, M., 2015. A review of sedimentation and preferred Solutions at Al-Ashkarah Fishery Port, Sultanate of Oman, *5th International Conference on Estuaries and Coasts, ICEC*, 165-174.

USACE, 1984. Shore Protection Manual. Department of the Army, U.S. Corps of Engineers, Washington, DC 20314.

Sazeh Pardazi Iran (SPI), 2007. Engineering study of water intake system of Paresar power station, sediment studies, *Report to MAPNA MD-2*, 29 pp.